Simultaneous detection of acoustic emission and Barkhausen noise during the martensitic transition of a Ni-Mn-Ga magnetic shape-memory alloy

Jordi Baró,[1] Steve Dixon,[2] Rachel S. Edwards,[2] Yichao Fan,[2] Dean S. Keeble,[2] Lluís Mañosa,[1] Antoni Planes,[1] and Eduard Vives[1]

[1]*Departament d'Estructura i Constituents de la Matèria, Facultat de Física, Universitat de Barcelona, Martí i Franquès 1, E-08028 Barcelona, Catalonia, Spain*

[2]*Department of Physics, University of Warwick, Coventry, CV4 7AL, United Kingdom*

(Received 5 August 2013; published 20 November 2013)

We present simultaneous measurements of acoustic emission and magnetic Barkhausen noise during the thermally induced martensitic transition in a Ni-Mn-Ga single crystal. The range where structural acoustic emission avalanches are detected extends for more than 50 K for both cooling and heating ramps, with a hysteresis of ∼10 K. The magnetic activity occurs during the structural transition, exhibiting similar hysteresis, but concentrated in the lower half of the temperature range. Statistical analysis of individual signals allows characterization of the broad distributions of acoustic emission and Barkhausen amplitudes. By studying the times of arrival of the avalanche events we detect the existence of correlations between the two kinds of signals, with a number of acoustic emission signals occurring shortly after a Barkhausen signal. The order of magnitude of the observed delays is compatible with the time needed for the propagation of ultrasound through the sample, showing correlation of some of the signals.

DOI: 10.1103/PhysRevB.88.174108 PACS number(s): 64.60.av, 81.30.Kf, 75.60.Ej, 43.40.Le

I. INTRODUCTION

Acoustic emission[1,2] (AE) is a characteristic feature of martensitic transitions, originating from displacement discontinuities across propagating interfaces.[3,4] The emitted pulses, typically detected in the ultrasonic frequency range, carry temporal and spatial information which characterizes the evolution of the internal strain field (order parameter) during the externally driven transformation process. AE is usually observed to occur as an intermittent sequence of temporal impulses, or avalanches, which are associated with the local strain discontinuities. The standard explanation for the AE behavior is that the system evolves by relaxing from one metastable state to another, within a complex energy landscape that characterizes the two-phase coexisting region. The statistical distribution of the energy and/or duration of avalanches can be obtained from AE measurements, and provides relevant information concerning the dynamics within this complex energy landscape. In some cases, these distributions are found to follow a power law, indicating the absence of characteristic scales for the avalanches. This situation defines the so-called avalanche criticality.[5,6]

Magnetic shape-memory alloys are a class of multiferroic materials which undergo a martensitic transition, with strong interaction between structure and magnetism.[7,8] A prototypical case is the Ni-Mn-Ga alloys, which, within the ferromagnetic phase, display a structural transition that can be induced either by changing temperature or by applying an external magnetic field.[9,10] In this class of materials, avalanches associated with the magnetic degrees of freedom are also expected to occur. Such avalanches in ferromagnetic materials are known as magnetic Barkhausen noise (BkN) when induced by a changing external magnetic field, but they may also be induced by temperature changes; note that this BkN is purely magnetic. Therefore, one would naively expect that AE should be accompanied by some kind of BkN in these materials.

The existence of magnetic BkN has been reported to occur in a Ni-Mn-Ga magnetic shape-memory alloy,[9,10] although it has been denoted as the "magnetic transition spectra." The measurements seem to indicate that the magnetic changes are a secondary effect, following the structural ones. However, the BkN events were measured as occurring at temperatures well below the temperatures at which the structural transition nominally occurs, according to standard calorimetric measurements. Thus, the authors suggest that there exist no coupled dynamic effects between structural and magnetic relaxation events.[9,10]

In the present paper we investigate further the possibility of a magnetoelastic interaction. We combine calorimetric measurements with simultaneous detection of BkN and AE signals, allowing a much better understanding of both kinds of avalanches and any correlations between the two.

II. EXPERIMENTAL

A sample with composition $Ni_{50.5}Mn_{29.5}Ga_{20.0}$ (valence electron concentration per atom $e/a = 7.71$), cut from the single crystal sample 3 described in Ref. 11, was studied. The sample has a disklike shape, with height $h = 2.5$ mm, and flat surfaces perpendicular to the (100) direction of the cubic high temperature phase. The faces are both elliptical, with maximum and minimum diameters $\Phi_{max} = 15$ mm and $\Phi_{min} = 13$ mm. Previous calorimetric measurements on a different specimen taken from the same crystal allowed determination of the Curie temperature as $T_c = 365$ K, and the structural transition temperature $M_s = 345 \pm 5$ K on cooling.[11]

The martensitic structure, as determined by x-ray diffraction on a powder specimen at a temperature of 193 K, was previously described as tetragonal nonmodulated ($L1_0$),[11] but the position of the dip in the TA_2 phonon branch (corresponding to a bulk rather than powder sample), obtained by inelastic neutron diffraction at high temperatures, suggests that the most stable martensitic structure should be close to monoclinic (14M or possibly 10M). The chemical composition

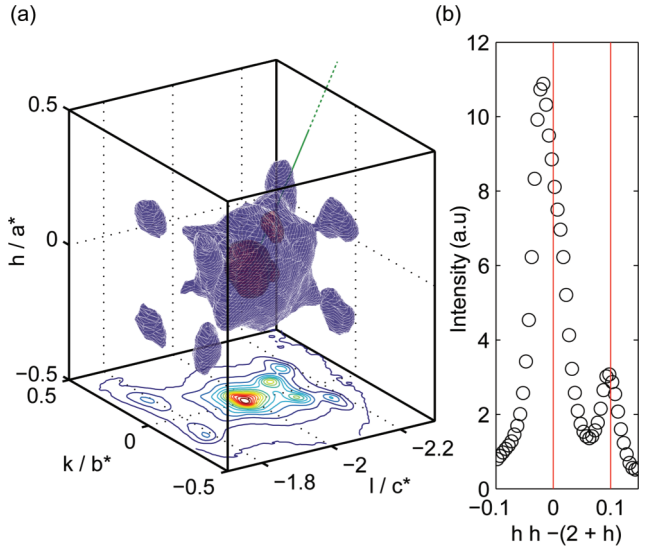

FIG. 1. (Color online) Diffraction data showing a 10M modulated structure. (a) 3D reconstruction of the $(00\bar{2})$ reflection of the $L1_0$ cell, and projection onto the [100] plane. Eight equivalent modulation directions are observed, with the $(11\bar{1})$ direction highlighted in green. (b) Intensity along the $(11\bar{1})$ direction through the $(00\bar{2})$ reflection of the $L1_0$ cell. The red lines represent the expected $(hh\overline{2+h})$ values for tenfold modulation along this direction, i.e., at $h = 0$ and $h = 0.1$. The existence of a peak at $h = 0.1$ confirms the tenfold modulation as expected for the 10M form of Ni-Mn-Ga.

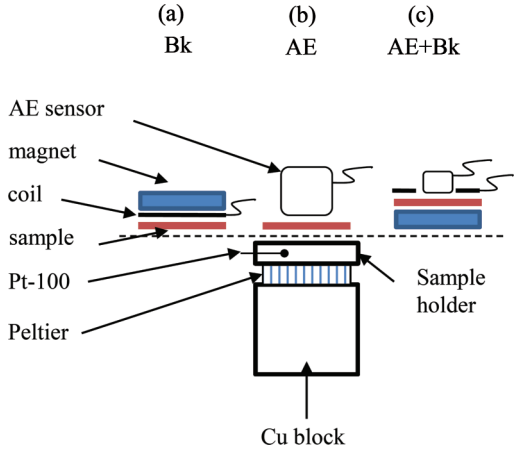

FIG. 2. (Color online) Schematic diagram of the experimental setup used for the study of (a) BkN, (b) AE, and (c) both AE and BkN simultaneously.

also indicates that the sample sits in a region of the phase diagram where the three structures ($L1_0$, 14M, and 10M) have very similar free energy.[12]

To confirm the crystal structure of the material in bulk crystal form at room temperature, a small section of the sample (of several mm dimensions on each side) was mounted on a Gemini R CCD x-ray diffractometer. Expanded regions of reciprocal space were collected in reflection geometry from one major face of the slice of the sample, using MoKα radiation at room temperature. The data were indexed, and reconstructed volumes of reciprocal space were extracted using CrysAlisPro (Agilent Technologies).

The diffraction data clearly reveals a modulated structure, with a tetragonal subcell of dimensions $a = 4.109(4)$ Å and $c = 2.503(3)$ Å, consistent with the previously observed $L1_0$ cell.[13] The modulation of this structure was indexed as being along the $\{111\}$ directions of the $L1_0$ cell [Fig. 1(a)], and the modulation peaks were found to exist at a spacing of $0.1\times(111)$ from the parent subcell reflection [Fig. 1(b)], indicating a tenfold modulation consistent with the 10M phase.[13] Calorimetric measurements as a function of temperature exhibit features compatible with the existence of overlapping intermartensitic phase transitions, or variant rearrangement. Thus, on cooling between the high temperature cubic phase and the low temperature 10M monoclinic phase, there potentially exist other intermediate tetragonal or 14M phases. Such a behavior is not surprising for these Mn-rich alloys that potentially exhibit competition between ferromagnetic and antiferromagnetic interactions.

The experimental setup used for simultaneous detection of AE and magnetic BkN is shown schematically in Fig. 2. Temperature is controlled using a Peltier element, sandwiched between a large copper block and the sample holder, driven by a programmable power supply. This setup is capable of delivering a temperature range between 273 K and 393 K, at typical ramp rates of 0.5–2 K/min. Temperature is measured using a Pt-100 resistor embedded into the sample holder, with an estimated absolute error of less than 1 K.

Three different configurations of the upper part of the setup have been used, depending on whether the system measures primarily BkN signals, AE only, or both signals simultaneously. For the first case [Fig. 2(a)], the sample is placed on the sample holder coupled with thermal conducting paste in order to ensure a good thermal contact. A flat spiral coil with 60 turns, covering the full sample, is placed on the top surface (this is the pick-up coil). The coil is 0.3 mm thick, made with 0.1 mm diameter copper wire, embedded in epoxy resin, and is AC coupled to a 60 dB gain preamplifier via a 10 μF capacitor. Magnetic flux transients through the coil windings are detected as induced voltage into the input of the preamplifier. The Curie peak from the sample was visible regardless of the bias magnetic field configuration, but a bias magnetic field from a permanent magnet (~0.07 T, 18 mm diameter) was used in order to observe BkN signals above the noise floor at other temperatures. This bias magnetic field was sufficiently weak to avoid broadening of magnetic phase transitions, but strong enough to enhance the magnetic BkN signal detection efficiency.

For AE measurements [Fig. 2(b)], the coil and permanent magnet are replaced by an AE transducer (R15LT from Mistras Group), acoustically coupled to the sample with a thin layer of vaseline. This is done to reduce the influence of the sample surface boundary conditions and the acoustic impedance mismatch. The AE transducer also uses a 60 dB gain preamplifier. For simultaneous detection of AE and BkN signals [Fig. 2(c)], the permanent magnet is placed between the sample holder and the sample. The coil is substituted by another spiral coil with a 7 mm diameter hole in the center, allowing a small AE sensor (pico-HF 1.2) to contact the sample. This second coil has a 1.5 μF capacitor in series. Some measurement sensitivity is sacrificed in this configuration, due

to a smaller number of turns in the BkN sensor, and the smaller AE sensor footprint. There is also a small lag between the actual sample temperature and the measured temperature in the sample holder, because the permanent magnet is a relatively poor thermal conductor.

The full setup is placed into a Faraday cage specifically designed for this experiment, consisting of an outer cubic steel box (600 mm sides, 4 mm thick), and an inner cubic copper box (400 mm sides, 3 mm thick). The preamplifiers are placed inside the cage and are connected with grounded coaxial cables to the external acquisition setup. The four wires from the Pt-100 and the connections of the Peltier element are individually covered with a coaxial ground, and the Faraday cage provides at least 30 dB attenuation of external electromagnetic interference in the frequency range of interest.

The signals from the preamplifiers are input to a PCI-2 acquisition system from Mistras Group, with a 10 MHz sampling rate. Software bandpass filters are used: 100 kHz – 2 MHz for AE, and 1 kHz – 3 MHz for BkN. Individual AE and BkN events are defined in the following way: events start when the signal crosses a threshold (chosen at 21 dB for BkN and 23 dB for AE) and finish when the signals have remained below threshold for more that 100μs. The amplitude A (in integer dB) is measured as the maximum voltage of the digitized signal.

Magnetic and acoustic activities are measured by counting the number of events per degree of temperature change, and for each individual event the amplitude in dB is determined. For the case of AE, it is also possible to measure the duration of the signals and to determine the energy of each individual event by fast integration of the squared voltage signal. Statistics for these quantities will be presented in the following sections.

Some of the event signals were also recorded at a 500 MHz analog bandwidth using a Tektronix TDS 520B oscilloscope, with a 1 GHz sampling rate. Calorimetric measurements of the studied specimen have also been done using a differential scanning calorimeter, with cooling and heating at approximately 0.4 K/min.

III. RESULTS AND DISCUSSION

A. Magnetic and acoustic activity

Figure 3 shows the magnetic activity recorded during cooling (upper panel) and heating (lower panel) ramps. As can be seen, when the Curie point (nominally at 365 K) is crossed from high temperatures to low temperatures there is an enhancement of the activity, that then smoothly decreases upon further cooling. On top of this feature, there is a clear peak centered around 305 K that exhibits some hysteresis between cooling and heating. The signals around the Curie point have very small amplitudes (see later statistical analysis), and are not detected if the threshold is slightly increased; Fig. 3 shows the effect of a threshold increase of only 1 dB as dashed lines, and only the peak around 305 K remains. These low amplitude signals are therefore likely to be an increase of the background noise due to sample magnetization.

Figure 4 shows the overlap of the calorimetric signal (continuous line), and the filtered magnetic (BkN) and the acoustic (AE) activities (continuous and dashed histograms,

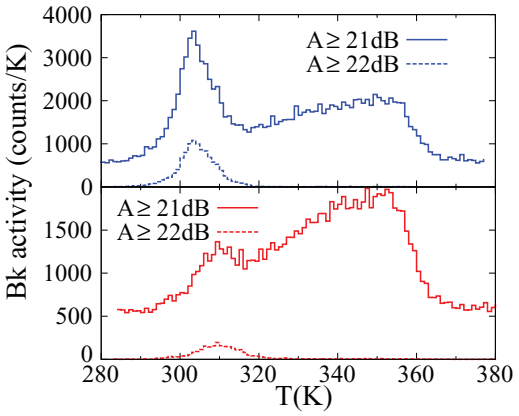

FIG. 3. (Color online) (a) Magnetic BkN activity as a function of temperature during cooling (upper panel) and heating (lower panel) ramps at 2 K/min. Dashed lines correspond to the histograms obtained after filtering out signals with amplitudes A less than or equal to 21 dB.

respectively). The activities were obtained in separate experiments using the first two experimental setups described above. The calorimetric signals exhibit a clear change in slope associated with the Curie point close to 365 K, in agreement with previous measurements.[11] The curve also exhibits a broad and irregular peak structure, with a maximum around 319 K on heating, and around 305 K on cooling, associated with the structural transition. This broad peak is not symmetric and exhibits an internal structure that can be described by the overlap of three peaks. Such a compound structure suggests that there could indeed be an overlap of martensitic and intermartensitic transitions, specifically cubic-tetragonal, cubic-monoclinic and tetragonal-monoclinic.

By tracing a tangent baseline (indicated by dashed straight lines in Fig. 4) one can determine the area below the

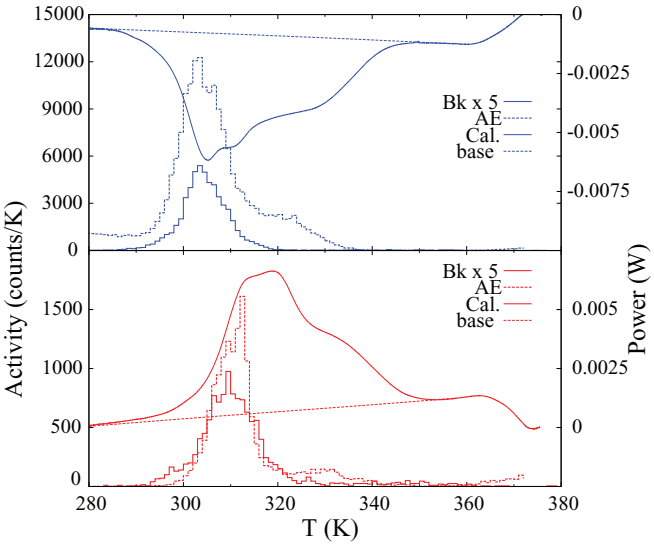

FIG. 4. (Color online) Calorimetric curve (continuous line, in W, right scale), AE activity (dashed histogram, in counts/K, left scale) and BkN activity (continuous histogram, in counts/K, left scale) for heating (bottom) and cooling (top) runs. The straight dashed lines show the baseline for integration of the calorimetric curve. The BkN activity has been multiplied by a factor of 5 to clarify the picture.

TABLE I. Summary of the positions of the initial, peak, and final temperatures, detected by AE, BkN, and calorimetry.

	Technique	T_{low} (K)	T_{peak} (K)	T_{high} (K)
Heating	Calorimetry	292	319	345
	AE	293	312	343
	BkN	293	310	323
Cooling	Calorimetry	290	305	342
	AE		303	336
	BkN	288	303	318

calorimetric curve and obtain the latent heat L associated with the first-order transition, with the data here giving a value of $L = 6.2 \pm 0.1$ J/g. The estimated measurement error includes the discrepancies between cooling and heating. This value is in agreement with previous measurements of Ni-Mn-Ga alloys transforming to monoclinic and tetragonal phases.[12] By determining the position of the temperatures T_{low} and T_{high} at which 1% and 99% of the total area are reached, the values of the start and end of the transition for both cooling and heating can be found. The values are reported in Table I.

The AE activity histogram (dashed) indicates the number of events detected above threshold on bins with a width of 1 K. It exhibits, as expected for athermal martensitic transitions, a behavior very similar to the calorimetric curve. When cooling, the starting point of the transition can be determined at 336 K, when the curve exceeds the background noise level. The end of the activity is more difficult to locate because few acoustic events occur for very low temperature values, and these are difficult to distinguish from the increase in the noise level that also occurs in blank measurements. This is an expected occurrence in thermally induced martensitic transitions; some domains of the high temperature cubic phase remain pinned due to internal stress and require very large undercooling to be transformed. The values of the estimated transition temperatures (the temperature where activity exceeds background noise) are also shown in Table I.

In contrast to the AE curves, the magnetic BkN activity histogram (continuous lines) shows a more symmetric peak, situated in the lower temperature region of the structural transition and with a much lower value for T_{high}. The limiting temperatures T_{low} and T_{high} and the position of the maximum activity are also shown in Table I. The calorimetry, AE, and BkN all reveal a certain hysteresis with temperature. A quantitative estimation of this can be obtained from the shifts of the peak temperatures on comparing cooling and heating, with $\Delta T = 14$ K from calorimetry, 9 K from AE, and 7 K from BkN.

The results presented so far suggest that, when cooling, the transition proceeds as follows: First, there are a number of structural changes (nucleation of martensitic domains) giving AE and latent heat. After enough structural changes have occurred, the magnetic domain walls start to move and adapt to the new structural configuration, giving BkN signals. The process is reversed during heating, with simultaneous reorganization of the magnetic domains occurring with the first structural transformations, and the magnetic BkN signals stopping well before the structural transition to the cubic phase is complete. This picture is in partial disagreement with what has been reported previously in the literature,[9] where in a Ni-Mn-Ga sample it was suggested that there is a magnetic reorganization at temperatures clearly below the structural transition. The reason behind this disagreement could be due to the different composition of the sample, or to the fact that the calorimetric measurements in Ref. 9 were done only on a small portion of the sample used for the BkN measurements, or due to other BkN sources. Thus, the width of the structural transition was most probably underestimated. In this paper the same sample is used for BkN, AE, and calorimetry, giving a more reliable comparison.

B. Magnetic signals

Figure 5(a) shows an example of a BkN signal measured using the PCI-2 acquisition system at about 318.5 K during a heating run. BkN signals in this material always consist of a sharp spike (either positive or negative) followed by a damped tail with the opposite sign. This characteristic shape has been confirmed by high resolution capture using an oscilloscope. When registered by the PCI-2 acquisition system (limited to 3 MHz analog bandwidth and a 10 MHz sampling rate) the signals display a wide range of amplitudes spanning more than a decade (from 21 dB to 40 dB). Automatic measurement of signal duration is difficult because the estimated value dramatically changes depending on whether or not the second oscillation crosses the threshold. Reliable signal durations

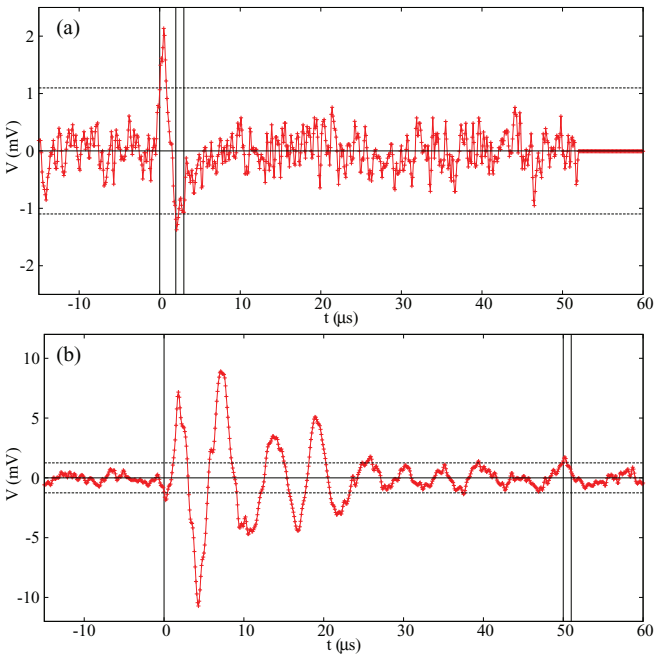

FIG. 5. (Color online) Examples of (a) a BkN signal (at 318.5 K) with 26 dB amplitude and 2 μs duration and (b) an AE signal (at 332.9 K) with 40 dB amplitude and 50 μs duration, as recorded by the PCI2 system at 10 MHz during heating runs. The horizontal lines indicate the thresholds (21 dB for BkN and 23 dB for AE). The vertical lines indicate the measured beginning of the signals and the double vertical line the end of the signal. The separation of the two ending lines indicates the resolution of 1 μs in the determination of the duration.

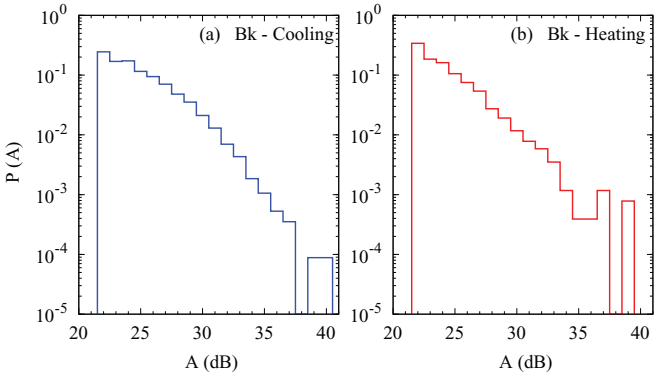

FIG. 6. (Color online) Log-log histograms revealing the amplitude distribution of the BkN signals for (a) cooling runs and (b) heating runs. Only amplitudes above or equal to 22 dB have been considered.

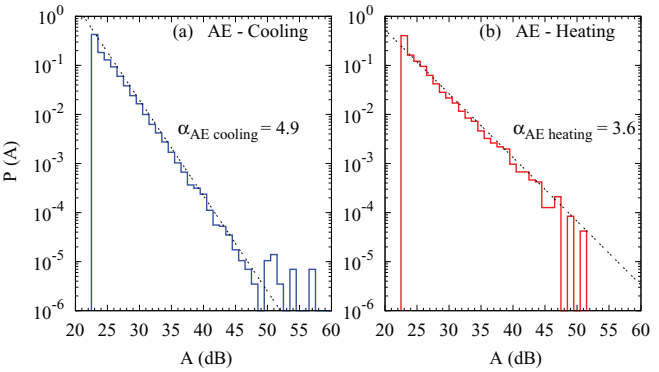

FIG. 8. (Color online) Log-log histograms corresponding to the amplitude distribution of the AE signals for cooling (a) and heating (b). Dashed lines correspond to $\alpha_{AE} = 4.9$ and $\alpha_{AE} = 3.6$, respectively.

measured by manual inspection, corresponding to the width of the sharp spike, are always restricted within a short range of 1–6 μs.

Figure 6 gives the histogram $P(A)$ of the amplitudes of the BkN signals registered during the full cooling and heating runs. The vertical axis corresponds to the fraction of signals detected with a given amplitude A (in dB). The distributions are quite broad and one would be tempted to associate them with a power-law probability $P(A) \sim A^{-\alpha_{BkN}}$, decaying with an exponent $\alpha_{BkN} \sim 4 - 5$. A more detailed analysis can be performed by using a maximum likelihood (ML) method, as explained in references.[14,15] This procedure renders an estimation of the exponent α_{BkN} which is independent of the data representation (bins, axis, etc.). Moreover, in order to test the robustness of the power-law hypothesis, the exponent is fitted to a restricted subset of the recorded data, above an imposed threshold $A_{\min}$. One expects that the exponent should be independent of the threshold, at least for one decade of A. In the present case, the fitted exponent α_{BkN} as a function of the lower threshold $A_{\min}$ is shown in Fig. 7. The plot reveals that the effective exponent generally increases with the threshold without any clear plateau. Thus, the data in Fig. 6 would be better described with an exponentially damped tail. This damping could have different origins; it could be a consequence of the fact that the sampling rate is not high enough to correctly detect the amplitude of the spikes, or due to distortions associated with the detection setup, or lack of statistics.

C. Acoustic signals

An example of an AE signal is shown in Fig. 5(b). Here, the signals exhibit typical behavior for AE pulses from structural transitions, when detected by piezoelectric transducers. Amplitudes range from 23 dB to 60 dB with durations from 1 to 3000 μs. Figure 8 shows histograms of the amplitudes recorded throughout the transition. Attempts to separate the statistical behavior in different regions within the transition have not rendered relevant data. Instead, the ML fit of the exponent α_{AE} as a function of the lower threshold shown in Fig. 9 reveals a plateau covering at least one decade, showing its power-law behavior. The obtained values are $\alpha_{AE} = 3.6$ for heating and $\alpha_{AE} = 4.9$ for cooling.

These values are unexpectedly high compared with previous measurements reported in the literature. Perez-Reche *et al.*[16] studied the α_{AE} exponent for a $Ni_{52.0}Mn_{23.0}Ga_{25.0}$ sample transforming, on cooling, to a monoclinic structure 10M, preceded by a premartensitic transition. They obtained a value of $\alpha_{EA} = 2.34 \pm 0.15$ but distorted with an exponential damping. In 2009, Ludwig *et al.*[17] studied a sample with the same composition ($Ni_{52.0}Mn_{23.0}Ga_{25.0}$), looking at the

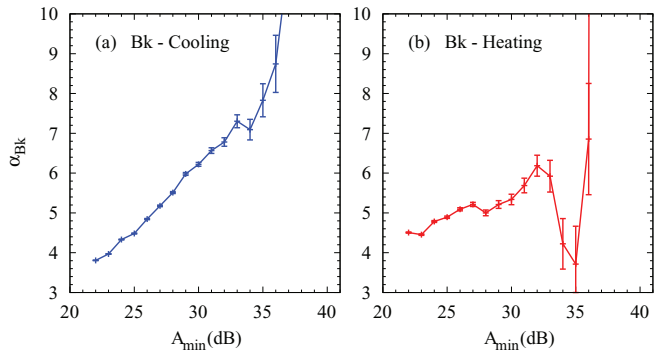

FIG. 7. (Color online) Power law exponent α_{BkN}, fitted with the maximum likelihood method to the amplitudes of the BkN pulses as a function of the lower amplitude threshold $A_{\min}$.

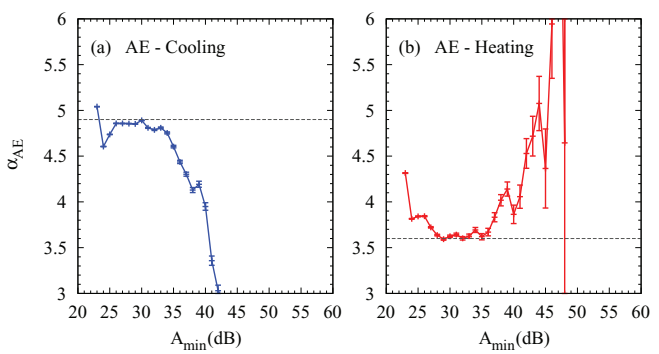

FIG. 9. (Color online) Power law exponent, fitted with the ML method to the amplitudes of the AE signals, as a function of a lower threshold $A_{\min}$.

behavior as a function of applied magnetic field. The extrapolation of their data to zero field (taking into account the fact that there was a small applied load) is compatible with a value of 2.9 ± 0.1 for both heating and cooling runs. Recently, Niemann *et al.*[18] studied a $Ni_{50.4}Mn_{27.9}Ga_{21.7}$ sample, transforming to a monoclinic 10M structure, as a function of an applied external uniaxial stress. They obtained a power-law exponent for the AE energy (E) distributions during heating runs at zero stress of $\epsilon_{AE} = 1.9 \pm 0.1$. Assuming a relationship of the form $E \sim A^2$, this exponent would correspond to a value of $\alpha_{AE} = 2\epsilon_{AE} - 1 = 2.8 \pm 0.2$. Thus the values from the recent literature point towards a common exponent close to $\alpha_{AE} \sim 2.9$ for cubic-monoclinic transformations in Ni-Mn-Ga. Similar values of $\alpha_{AE} \sim 3$ have been reported for Cu based alloys transforming to monoclinic structures.[5]

It has been suggested[19,20] that the exponents α_{AE} and ϵ_{AE} characterizing the power-law distributions of amplitudes and energies of the avalanches in structural transitions correlate with the variant multiplicity of the low temperature phase (given by the ratio of the number of symmetry operations in the high temperature phase to those in the low temperature phase); the greater the number of low temperature variants, the more freedom the system has to find a transformation path to any given metastable domain. The greater the number of possible transformation paths, the easier it will be to find low free-energy barriers, and consequently a larger fraction of avalanches will have lower energies instead of high energies (i.e., a larger power law exponent). This idea also fits with the exponents $\alpha = 2.26$ found for $Fe_{68.8}Pd_{31.2}$ alloys[21] transforming from cubic to tetragonal structures with multiplicity 3.

The sample used here has a different composition to the Ni-Mn-Ga alloys studied previously. However, irrespective of whether the low temperature phase is tetragonal (three variants) or monoclinic (12 variants), the values found for the exponent are much higher than expected. The calorimetric curves (Fig. 4) show a triple peak structure, suggesting that there could be some intermartensitic structural changes or variant rearrangement. Note that for both heating and cooling runs there is AE activity, not only below the maximum of the main calorimetric peak, but there is significant activity from the beginning of the calorimetric signals. Therefore, one can speculate that the large value of α_{AE} could be associated with the fact that in the composition studied, tetragonal and monoclinic (10M and 14M) structures have similar free energies. This suggests that the free energy landscape is very flat, displaying many shallow minima with almost equivalent energies. The number of possible dynamic paths connecting a cubic domain to a final domain in the martensitic structure is therefore very degenerate. For example, if we accept avalanche paths from cubic to monoclinic, involving also intermartensitic tetragonal changes, we obtain $3 \times 12 = 36$ available dynamic trajectories. This large number of degrees of freedom will justify the fact that most of the avalanches are very small, rendering a high exponent.

D. Correlations

Simultaneous detection of both the AE and BkN signals enables one to study the correlations between the two

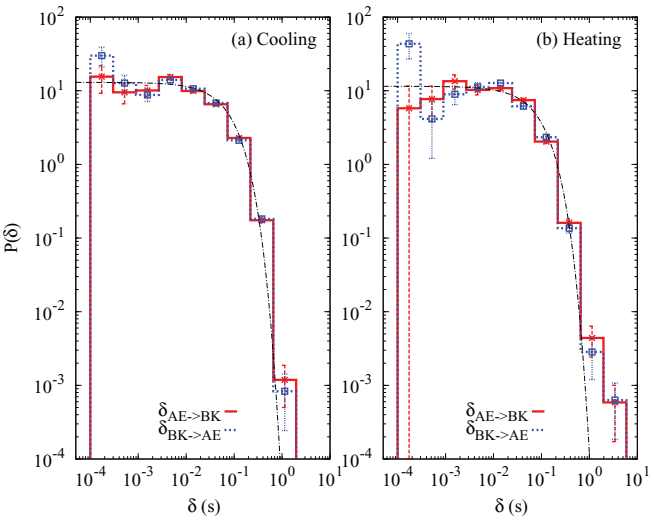

FIG. 10. (Color online) Distribution of the delays between consecutive AE → BkN signals and BkN → AE signals in a log-log plot for cooling (a) and heating (b) runs. Bins correspond to a factor ×3 (9.54 dB). The lines correspond to an exponential behavior $P(\delta) \sim \exp(-\delta\lambda)/\lambda$ with $\lambda = 11.5\ s^{-1}$ for heating and $\lambda = 13\ s^{-1}$ for cooling.

phenomena. It could be argued that the BkN coil used in this work could also detect AE through the same mechanisms as electromagnetic acoustic transducers (EMATs).[22] However, both the Lorentz and magnetostriction EMAT coupling efficiencies are low, as the applied bias magnetic field is very weak. If such signals were being detected, one would expect the BkN signals to follow closely the AE signals, with very similar values for T_{low}, T_{peak}, and T_{high}. This is not observed, and there are regions in temperature (see, e.g., Fig. 4) where only AE signals are measured with no detection on the BkN sensor. Furthermore, the behavior shown in Figs. 6 and 8 and also the fits to a power law distribution for BkN and AE (shown in these figures) are different. Therefore, the EMAT coupling mechanism can be considered negligible, and the coil acts primarily as a BkN sensor. Using an elongated sample and optimized solenoidlike coil geometry, the magnetic BkN signal at similar temperatures can be detected with sufficient signal to noise ratio without needing the bias magnetic field.

In the temperature interval where the BkN activity is high, the time delays δ between pairs of consecutive signals of different origin (i.e., AE signals followed by a BkN signal or BkN signals followed by AE signals) have been analyzed. If the two processes were completely uncorrelated, the distribution of delays would be the same for both cases. The results are shown in Fig. 10. Both histograms are indistinguishable for large values of δ, where events are clearly uncorrelated. However, for short delays (first bin), the data show an excess of counts above the error bars for the number of BkN signals followed by AE, compared to AE followed by BkN. This means that there is a tendency for certain AE signals to be correlated and slightly temporally delayed, after a previous BkN pulse. In the same figure, we also represent (dashed line) the exponential behavior that one would expect if the occurrence of BkN and AE signals were uncorrelated random processes. As can be seen, the observed increase in the first

bin also deviates from the expected flat behavior for small δ. Slight deviations in the large δ region can be explained through variations of the rate during the transition (nonhomogeneous character of the random processes).[23]

The AE events were detected using a piezoelectric transducer, physically coupled to the sample surface via a thin layer of vaseline. The AE sensor is only sensitive to the out-of-plane component of the acoustic vibrations, and hence AE events with energy predominantly in the in-plane direction at the sensor will likely be missed. However, AE events originating at any point in the sample with a sufficiently large out-of-plane component at the sensor will be detected, each with their own acoustic propagation delay corresponding to the physical distance traveled before reaching the AE sensor. The magnetic BkN events were electromagnetically coupled to the pick-up coil. While the electromagnetic propagation delay of these signals in air is negligible, the propagation delay inside the sample is not, because the Ni-Mn-Ga sample has a non-negligible electrical conductivity and magnetic permeability. For the same reason, the pick-up coil is only sensitive to BkN signals originating near the sample surface, due to the shallow electromagnetic skin depth.

It is expected that any structural change in the sample should result in a simultaneous reorganization of the magnetic microstructure, driven by the strong changes in the magnetocrystalline anisotropy. Therefore, a correlation between AE and BkN signals is not unexpected. Note that the observed correlation between the BkN events which are detected shortly before AE events does not directly imply that magnetic changes cause structural changes; the two types of signals are detected via radically different physical mechanisms, each with their own influences on the detection time of the events, and the relative timing accuracy of the data acquisition system can also be a significant limitation. However, the observed correlation does indicate that at least some of the BkN and AE events share the same physical origin, with the AE signal recorded as slightly delayed. Similar delays were also observed during the recording of individual signals in preliminary experiments.[24]

IV. SUMMARY AND CONCLUSIONS

We have studied a Ni-Mn-Ga ferromagnetic shape memory alloy exhibiting a thermally induced martensitic transition. Calorimetric curves for both heating and cooling exhibit a multipeak structure indicating that the transformation path may involve intermartensitic transformations. This is not surprising, since for this composition the tetragonal and monoclinic structures exhibit similar free energies. The AE data indicates a temperature transition width of about 50 K, and the maximum AE activity occurs around 312 K for heating and 303 K for cooling, with a hysteresis of ~9 K. These features are in agreement with calorimetry results. The detection of BkN signals shows that the magnetic reorganization activity occurs in the low temperature half segment of the structural transition, with a smaller thermal range of about 30 K, exhibiting a similar hysteresis of ~7 K.

Statistical analysis of the two kinds of signals shows that the amplitudes are broadly distributed, but for the BkN case they exhibit a clear exponential damping. For AE, the fitted power-law exponents are very high ($\alpha_{AE} = 3.6$ for heating and $\alpha_{AE} = 4.9$ for cooling) compared with the expected values from considering measurements of similar structural transitions. The reason for such a high fraction of small avalanches may be due to the flat free energy landscape that allows for many degenerate dynamic transformation paths. Simultaneous detection of AE and BkN has allowed identification of some correlations between the time of arrival of the pulses from each mechanism. A number of AE signals arrive shortly after a BkN signal, and this delay could be attributed to the time needed for the propagation of ultrasound within the sample. These results show evidence for coupled dynamics between magnetic and elastic relaxations in ferromagnetic shape memory alloys. In order to gain a deeper understanding, measurements with increased time resolution are needed. Moreover, similar analysis for near-stoichiometric single crystals and/or using other metamagnetic shape memory alloys, such as Ni-Mn-In or Ni-Mn-Sn, would allow further insights.

ACKNOWLEDGMENTS

We acknowledge financial support for this work from the Spanish Ministry of Science (MAT2010-15114), and from the Royal Society (International Joint Project JP090474). XRD equipment was provided through the Science City Advanced Materials Project, with support from Advantage West Midlands and part funded by the European Regional Development Fund. R.S.E. and Y.F. thank the ERC for financial support (Grant No. 202735).

[1] C. B. Scruby, J. Phys. E **20**, 946 (1987).
[2] For a recent review see *Acoustic Emission Testing*. edited by C. U. Grosse and M. Ohtsu, (Springer-Verlag, Berlin-Heidelberg, 2008).
[3] E. Vives, J. Ortín, Ll. Mañosa, I. Ràfols, R. Pérez-Magrané, and A. Planes, Phys. Rev. Lett. **72**, 1694 (1994).
[4] E. Vives, I. Ràfols, Ll. Mañosa, J. Ortín, and A. Planes, Phys. Rev. B **52**, 12644 (1995).
[5] L. Carrillo, Ll. Mañosa, J. Ortín, A. Planes, and E. Vives, Phys. Rev. Lett. **81**, 1889 (1998).
[6] F. J. Pérez-Reche, E. Vives, Ll. Mañosa, and A. Planes, Phys. Rev. Lett. **87**, 195701 (2001).
[7] O. Söderberg, A. Sozinov, Y. Ge, S.-P. Hannula, and V. K. Lindroos, *Giant Magnetostrictive Materials*, in Handbook of Magnetic Materials, Vol. 16, edited by J. Buschow (Elsevier Science, Amsterdam, 2006), pp. 1–39.
[8] T. Kakeshita and K. Ullakko, MRS Bulletin **27**, 105 (2002).
[9] M. R. Sullivan, A. A. Shah, and H. D. Chopra, Phys. Rev. B **70**, 094428 (2004).
[10] J. N. Armstrong, J. D. Felske, and H. D. Chopra, Phys. Rev. B **81**, 174405 (2010).
[11] Ll. Mañosa, A. Planes, J. Zarestky, T. Lograsso, D. L. Schlagel, and C. Stassis, Phys. Rev B **64**, 024305 (2001).

[12]M. Acet, Ll. Mañosa, and A. Planes, *Handbook of Magnetic Materials*, Vol. 19, edited by K. H. J. Buschov (Elsevier B.V., Amsterdam, 2011).
[13]J. Pons, V. A. Cherneko, R. Santamarta, and E. Cesari, Acta Materialia **48**, 3027 (2000).
[14]A. Clauset, C. R. Shalizi, and M. E. J. Newman, SIAM Review **51**, 661 (2009).
[15]J. Baró and E. Vives, Phys. Rev. E **85**, 066121 (2012).
[16]F. J. Pérez-Reche, E. Vives, Ll. Mañosa, and A. Planes, Materials Science and Engineering A **378**, 353 (2004).
[17]B. Ludwig, C. Strothkaemper, U. Klemradt, X. Moya, Ll. Mañosa, E. Vives and A. Planes, Appl. Phys. Lett. **94**, 121901 (2009).
[18]R. Niemann, J. Baró, O. Heczko, L. Schultz, S. Fähler, E. Vives, Ll. Mañosa, and A. Planes, Phys. Rev. B **86**, 214101 (2012).
[19]M. L. Rosinberg and E. Vives, in *Disorder and Strain-induced complexity in Functional Materials*, edited by T. Kakeshita, T. Fukuda, A. Saxena, and A. Planes, Springer Series in Materials Science (Springer-Verlag, Berlin, 2013).
[20]A. Planes, Ll. Mañosa, and E. Vives, J. of Alloys Compd., doi:10.1016/j.jallcom.2011.10.082.
[21]E. Bonnot, Ll. Mañosa, A. Planes, D. Soto-Parra, E. Vives, B. Ludwig, C. Strothkaemper, T. Fukuda, and T. Kakeshita, Phys. Rev. B **78**, 184103 (2008).
[22]M. Hirao and H. Ogi, *EMATs for Science and Industry* (Kluwer Academic, Boston, 2003).
[23]J. Baró, A. Corral, X. Illa, A. Planes, E. K. H. Salje, W. Schranz, D. E. Soto-Parra, and E. Vives, Phys. Rev. Lett. **110**, 088702 (2013).
[24]E. Vives, D. Soto-Parra, A. Planes, Ll. Mañosa, R. Romero, R. S. Edwards, and S. Dixon, Solid State Phenomena **172-174**, 144 (2011).